Scripta Materialia 194 (2021) 113606

Contents lists available at ScienceDirect

Scripta Materialia

journal homepage: www.elsevier.com/locate/scriptamat

Ultrastability of metallic supercooled liquid induced by vibration

H. Zhao[a,b], F. Sun[a], X. Li[c], Y. Ding[b], Y.Q. Yan[a], X. Tong[a], J. Ma[c,*], H.B. Ke[a,*], W.H. Wang[a,b,d]

[a] Songshan Lake Materials Laboratory, Dongguan 523808, People's Republic of China
[b] College of Physics, Liaoning University, Shenyang 110036, People's Republic of China
[c] College of Mechatronics and Control Engineering, Shenzhen University, Shenzhen 518060, People's Republic of China
[d] Institute of Physics, Chinese Academy of Sciences, Beijing 100190, People's Republic of China

ARTICLE INFO

Article history:
Received 6 October 2020
Accepted 29 October 2020

Keywords:
Supercooled liquid
Ultrasonic vibration
Metallic glasses
Ultrastability

ABSTRACT

The range of supercooled liquid region (ΔT) is the key parameter for evaluating the thermal stability and glass-forming ability of metallic glasses. The enhancement of ΔT is of significance not only for the glass formation and stability, but also for their thermoplastic forming ability. Traditional approaches to increase ΔT are composition regulation or dynamical modulation, which are either time-consuming or difficult to be controlled. Here, through a high-frequency ultrasonic vibration treatment, we show that the ΔT of a La-based metallic glass can be significantly widened from 64 K to 83 K, around 30% increment. This behavior is physically originated from the denser atomic packing and a lower stable basin in the energy landscape induced by the ultrasonic vibration energy. This work might provide a ready route to stabilize the supercooled liquid and glass, and give an insight into the understanding of the glass-forming of amorphous materials.

A glass is a vitrified liquid with disorder atomic structure and metastable energy state [1–3]. Upon heating, the glass will enter into supercooled liquid above the glass transition temperature T_g, and then crystallized at a higher temperature T_x. The difference between T_g and T_x defines the range of supercooled liquid region (SLR) ΔT (i.e. $\Delta T = T_x - T_g$), which is an important parameter for evaluating the glass forming ability (GFA) and stability of a glass [4–7]. Compared to organic and oxide glasses, metallic glass (MG) has attracted extensive attention due to the excellent mechanical properties [8–10]. Since its discovery [11], researchers have dedicated to searching new MGs with good GFA and high stability [12–14]. Many MGs with large ΔT show good GFA have been exploited, such as $Pd_{40}Cu_{30}Ni_{10}P_{20}$ (ΔT ~ 79 K) [15], $Zr_{46.25}Ti_{8.25}Cu_{7.5}Ni_{10}Be_{27.5}$ (Vit4, ΔT ~ 105 K) [16]. On the other hand, the thermal stability of MGs is usually quantified by the range of ΔT. Generally, a larger ΔT means a higher thermal stability, which would benefit for the studies of thermodynamic or relaxation behavior and the measurements of the properties for undercooled liquids. On the technology side, a wider ΔT provide a better processing time window for the thermoplastic forming to fabricate high-precision and high-performance components [17,18], which would broaden the application filed of MGs. Thus, an effective method to tune ΔT will benefit for the deep understanding of GFA as well as the development and processing of glasses.

Many routes have been used to tune ΔT of MGs [19–23]. One of the common ways is to adjust the constituent elements of the alloy, i.e., increasing or decreasing the content of some elements, minor addition or microalloying [19,24,25]. For example, Al addition dramatically enhances the thermal stability and GFA of a $(Cu_{50}Zr_{50})_{100-x}Al_x$ system [19]. With 8% Al addition, the T_g and T_x increased about 30 K and 66 K, respectively. Meanwhile, the GFA was raised from 2 mm to 5 mm. However, such composition regulation is time-consuming and also difficult to be controlled. Annealing below T_g can slightly change ΔT, which is inefficient and causes embrittlement of MGs [20]. Recently, a number of ultrastable MGs have been prepared by magnetron sputtering (MS) or deposition techniques with extreme low deposition rate [21–23]. These MGs exhibit excellent thermal stability with higher T_g and T_x. For example, the ion beam assisted deposition can obtain a ultrastable amorphous $Cu_{50}Zr_{50}$ thin film which shows an increase of 60 K for the crystallization temperature [21]. The super-low vapor deposition can produce ultrastable glass with a substantial increase in the glass transition temperature T_g [22]. However, it was found that most ultrastable MGs show a narrower supercooled liquid region as compared with ordinary MGs. So far, how to increase ΔT of an existing system intrinsically without composition or dynamic modulation remains an open challenge.

In this work, an ultrasonic vibration (UV) method was introduced to treat a typical $La_{55}Al_{25}Ni_5Cu_{10}Co_5$ MG. It is shown that

---

[*] Corresponding authors.
E-mail addresses: majiang@szu.edu.cn (J. Ma), kehaibo@sslab.org.cn (H.B. Ke).

https://doi.org/10.1016/j.scriptamat.2020.10.048
1359-6462/

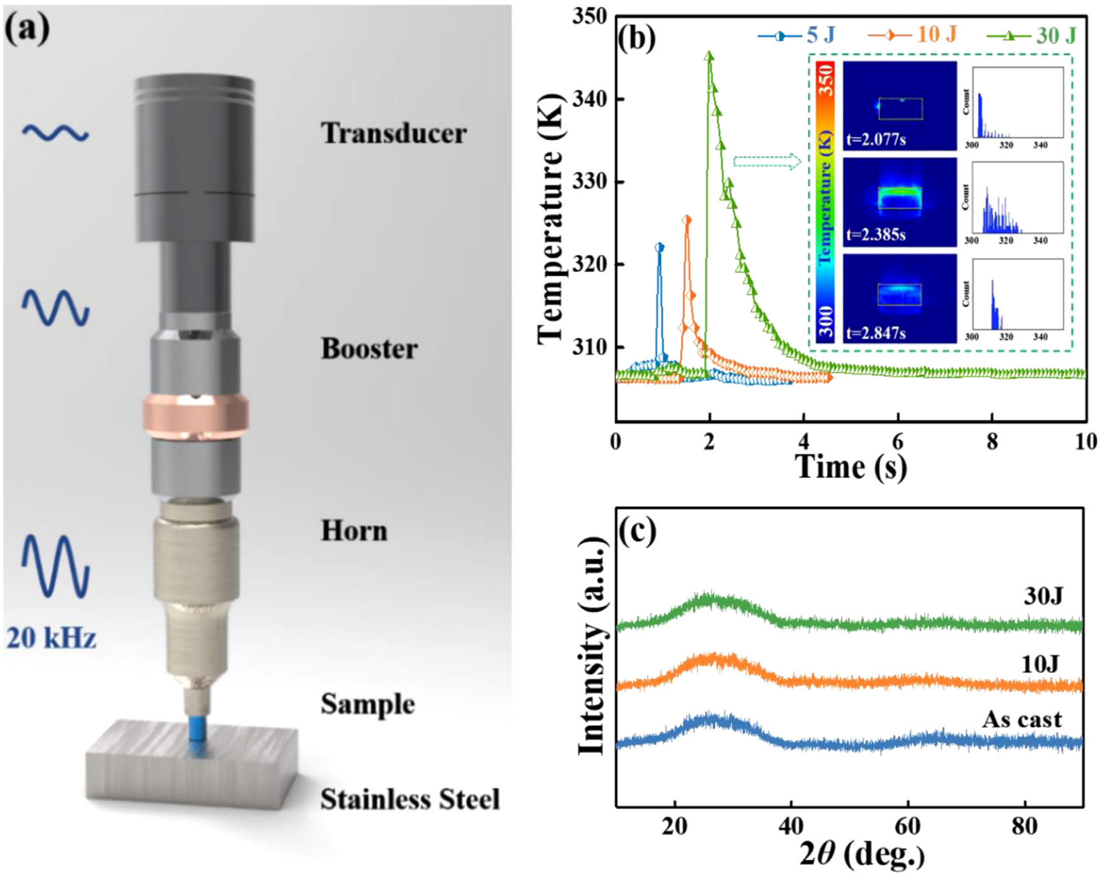

Fig. 1. Schematic diagram of ultrasonic treatment process and the variation of temperature and structure of the samples. (a) Ultrasonic vibration process sketch: ultrasonic vibration with 20 kHz is transmitted to the horn, and the horn exerts pressure and vibration on the sample. (b) The temperature variation of the samples obtains by high precision infrared thermometer during the ultrasonic process with different energy. The inset shows the temperature profile at different moments during UV at 30J. (c) XRD patterns for as cast sample and processed samples, which show no observed crystallization occurred.

both T_g and T_x can be manually tailored with different input energy. With appropriate input vibration energy, a maximum 19 K enhancement of ΔT, around about 30% increment can be achieved in the MG. The underlying physical mechanism of the phenomenon is rationalized in terms of vibration induced the disappearance of a high energy metastable structure with a relatively lower activation energy in MG. The results might provide an effective route to enhance the thermostability and widen ΔT of MGs, which would benefit for the thermoplastic processing and properties tailoring of MGs at the SLR.

The alloy ingots with nominal composition of $La_{55}Al_{25}Ni_5Cu_{10}Co_5$ were prepared by arc melting a mixture of elements with a purity of at least 99.9% under a Ti-gettered purified Ar atmosphere. To make sure a homogeneous composition, each ingot was remelted for five times. Cylindrical rods with diameters of 2 mm were prepared by copper-mold suction casting. Disks of 0.9 mm thickness were cut from the as cast rods and the ends were polished to ensure parallel surfaces. Then, these disks were processed by the ultrasonic vibrational equipment comprised a transducer for converting electrical energy to mechanical vibrations with a frequency of 20 kHz (see Fig. 1a for sketch) [26]. This equipment comprised a transducer for converting electrical energy to mechanical vibrations, a booster for amplifying the amplitude of vibrations, and a horn to transfer mechanical vibrations to the specimens. When the specimen was placed on the bottom mold, a minimal loading was preloaded to ensure close contact between the specimen and the horn. Then, different setting values of ultrasonic energies were applied to the specimen. Generally, the entire process only lasts for seconds depending on the energy input. The input energies of 5, 8, 10, 13, 15, 20 and 30 J were used. To obtain the thermal effect during the process, an infrared instrument with high precision of 1 K was used to monitor the temperature change. The phase structure of the as cast and UV processed specimens was confirmed by X-ray diffractometry (XRD, Bruke D8) with Cu Kα radiation. The samples for TEM observation were carefully prepared by the ion milling (Gatan 695) with 5 keV Ar ions at room temperature. High-resolution TEM images for as cast and UV processed samples are acquired using a FEI Talos F200X TEM. After the ultrasonic vibration treatment, the glassy structure of all the processed disks were re-examined by XRD and the thermal response were determined by differential scanning calorimetry (DSC, PE-DSC 8000) at a heating rate of 20 K/min. Different heating rate including 20, 40, 60, 80, 100 K/min were used for measuring the activation energy of crystallization peaks.

The schematic diagram of UV treatment is shown in Fig. 1a. Detail of the UV experiment can be found in the Methods section. This method had been used to weld metal sheets under low-temperature and low-pressure conditions [26]. Recently, it was introduced to welding and punching BMG without any crystallization [27–31]. The UV method was applied to $La_{55}Al_{25}Ni_5Cu_{10}Co_5$ MG. As shown in Fig. 1b, the temperature profiles of input energies up to 30 J indicate that the maximum temperature rise in the whole process was less than 40 K, which is far below its T_g of the MG. The X-ray diffraction (XRD) patterns before and after ultrasonic processed are shown in Fig. 1c. The broad diffraction peaks

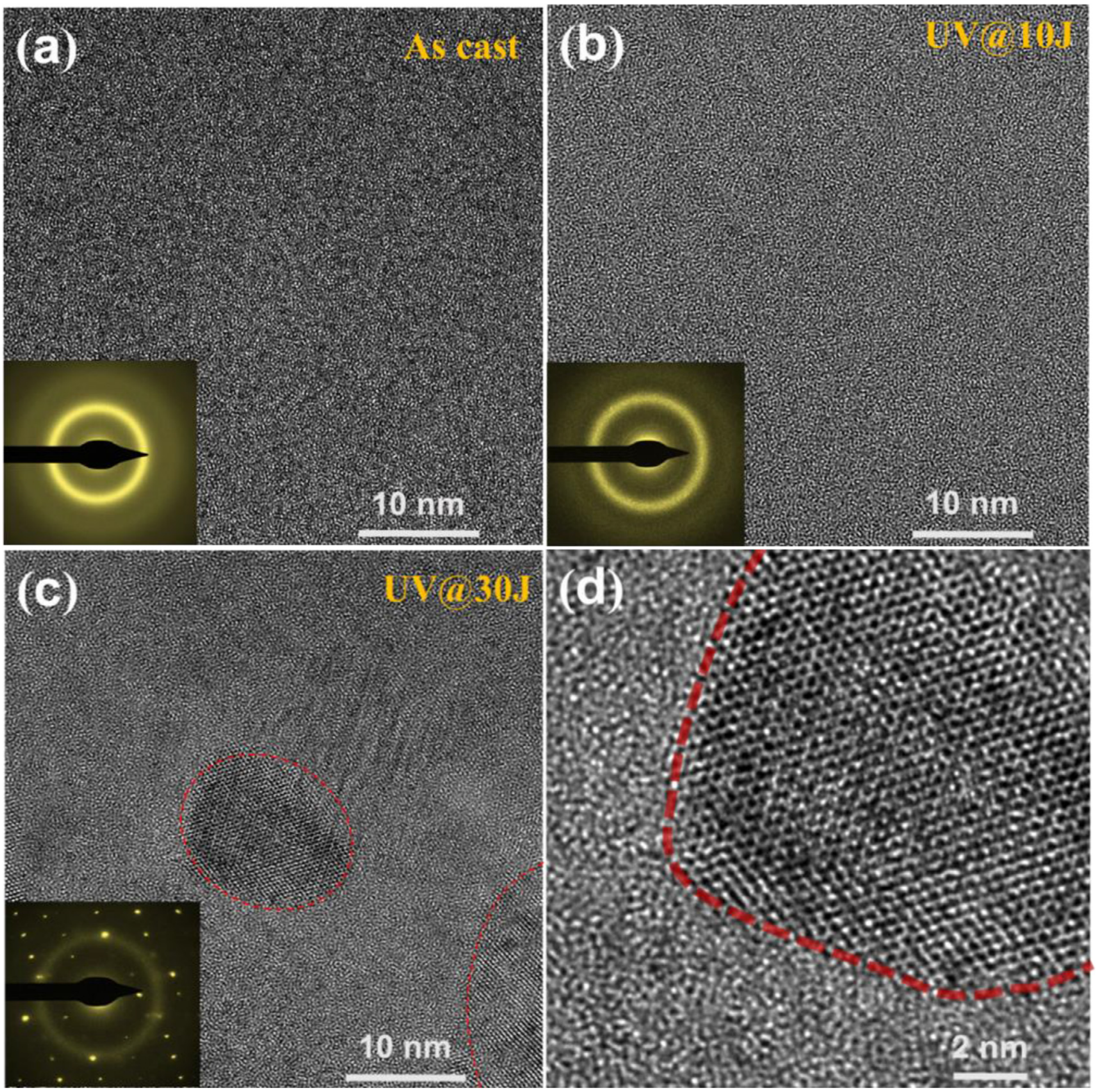

Fig. 2. Structure characterization of the as cast and UV processed samples. HRTEM of (a) as cast MG, (b) MG after UV treatment with energy of 10 J and (c) 30 J. Insets: SAED patterns taken from a large selected area. The red dotted line in (c) exhibits the nanocrystal embedded in the MG matrix. (d) An enlarged image of the atomic structure of the 30 J UV processed sample. The red dotted thick line shows a clear boundary between nanocrystal and amorphous matrix.

of the specimens mean that no observed crystallization happen after UV treatments.

To verify whether local crystallization exceeds the detection limit of XRD has intervened, we conducted high-resolution transmission electron microscopy (HRTEM) observation for both the as-cast and UV processed specimens, which is displayed in Fig. 2. When the energy is below 13 J, one can see disordered atomic structure accords with the diffractive halo-like selected area electron diffraction (SAED), indicating the fully glassy feature of both as cast sample (Fig. 2a) and UV processed sample with 10 J (Fig. 2b). However, with the UV energy of 30 J, nanocrystal with tens of nanometers can be observed in the MG matrix in Fig. 2c and d, accompanying with regular diffraction spots embedded in the diffraction halos.

The effect of UV on the thermal properties of the specimens was determined by differential scanning calorimetry (DSC). Fig. 3a shows the DSC scans of as cast and UV processed samples under different vibration energy using a heating rate of 20 K/min. One can see that the as cast sample presents a glass transition temperature at 452 K and two exothermic events characteristics of crystallization with the onset temperature T_x ~ 516 K, which is consistent with previous report [32]. As shown in Fig. 3a, the UV treatment obviously change crystallization temperature. With the increasing of input energy, the onset T_x of the UV processed MG specimens rises firstly and then returns to its initial value, while the T_g almost shows no change (see Table 1). Interestingly, only one exothermic event exists after UV treatment with input energy from 5 J to 15 J. The most significant change of T_x occurs at input energy of 10 J. In order to better capture the effect of UV treatment on the MG, Fig. 3b presents the variation of ΔT after processing with input energy of 10 J. It can be seen that the increment for ΔT is 19 K, which is the maximum value for UV treatments with various energy in this MG. Although the change of T_g is slightly, the disappearance of the first crystallization event leading to an increment of T_x from 516 K to 537 K, which in a nearly 30% enhancement in the width of the SLR.

To assess when partial structure alteration occurred during the UV process, the variation of ΔT and crystallization enthalpies ΔH_x were determined as listed in Table 1 and shown in Fig. 3c. One can see that ΔT has a significant increase compared with the as-cast state when the input energy is between 5 and 13 J, while the crystallization enthalpies ΔH_x keep unchanged. On the other hand, the value of ΔH_x is around 38 ~ 39 J/g when the energy is below 13 J, but an obvious reduction in ΔH_x only occurred when the input

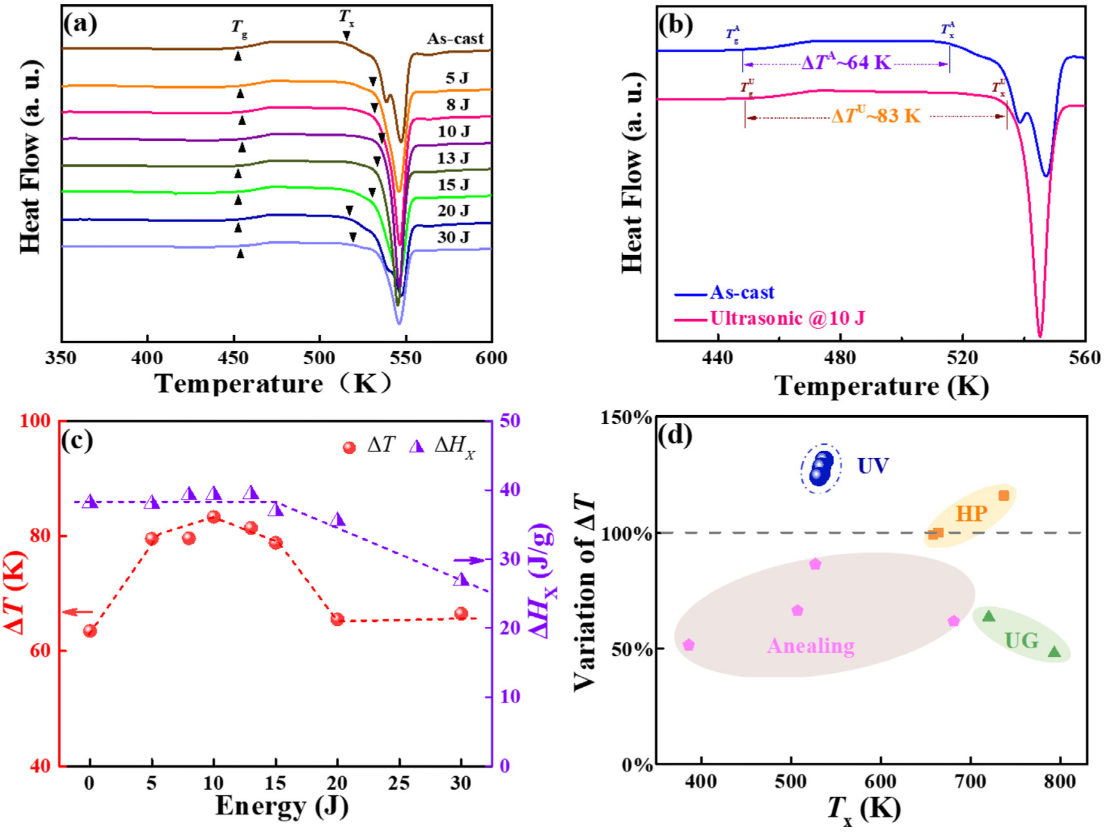

Fig. 3. The thermodynamic evolution behavior of La-based MG at various input energy. (a) The contrast DSC traces of as cast sample and UV samples with various input energies. For each alloy, the arrow pointing upwards indicates the glass transition temperature and the one pointing downwards indicates the crystallization temperature. (b) Comparison of ΔT for as-cast and UV processed sample with 10 J. (c) The ΔT and ΔH_x versus vibrational input energy. (d) Comparison of the variations in ΔT by different methods, including high pressure, deposition achieving ultrastable MG, sub-T_g annealing and ultrasonic vibration.

Table 1
Thermodynamic parameters of different MGs obtained by various preparation and treatment methods.

MG	Method	T_g (K)	T_x(K)	ΔT(K)	ΔH_x(J/g)	Ref.
$La_{55}Al_{25}Ni_5Cu_{10}Co_5$	Casting	452	516	64	38.1	This work
	UV (5 J)	453	532	79	38.0	
	UV (8 J)	454	533	79	39.2	
	UV (10 J)	454	537	83	39.3	
	UV (13 J)	452	534	82	39.4	
	UV (15 J)	452	531	79	36.9	
	UV (20 J)	452	517	65	35.5	
	UV (30 J)	453	519	66	26.8	
$Cu_{50}Zr_{50}$	Casting	670	713	43	/	[21]
	MS	/	772	/	/	
$Zr_{46}Cu_{46}Al_8$	Casting	689	773	75	/	[22]
	PVD	757	793	36	/	
$Zr_{65}Cu_{27.5}Al_{7.5}$	Casting	676	728	52	/	[23]
	PVD	687	720	33	/	
$Pd_{40.16}Ni_{9.64}Cu_{30.12}P_{20.08}$	Casting	566	653	87	/	[36]
	HP (10GPa)	572	658	86	/	
	HP (17GPa)	577	664	87	/	
$Zr_{41}Ti_{14}Cu_{12.5}Ni_{10}Be_{22.5}$	Casting	642	724	82	/	[37]
	HP (5GPa)	642	737	95	/	
$Zr_{41}Ti_{14}Cu_{12.5}Ni_{10}Be_{22.5}$	As-prepared	629	710	81	/	[38]
	Annealed at 623K	631	681	50	/	
$Au_{49}Cu_{26.9}Ag_{5.5}Pd_{2.3}Si_{16.3}$	Casting	424	507	83	40.2	[39]
	Annealed at 373K	452	507	55	40.2	
$Pt_{60}Ni_{15}P_{25}$	Casting	476	527	51	/	[40]
	Annealed at 461K	483	527	44	/	
$Ce_{68}Al_{10}Cu_{20}Fe_2$	Casting	343	411	68	/	[41]
	Annealed at 333K	351	386	35	/	

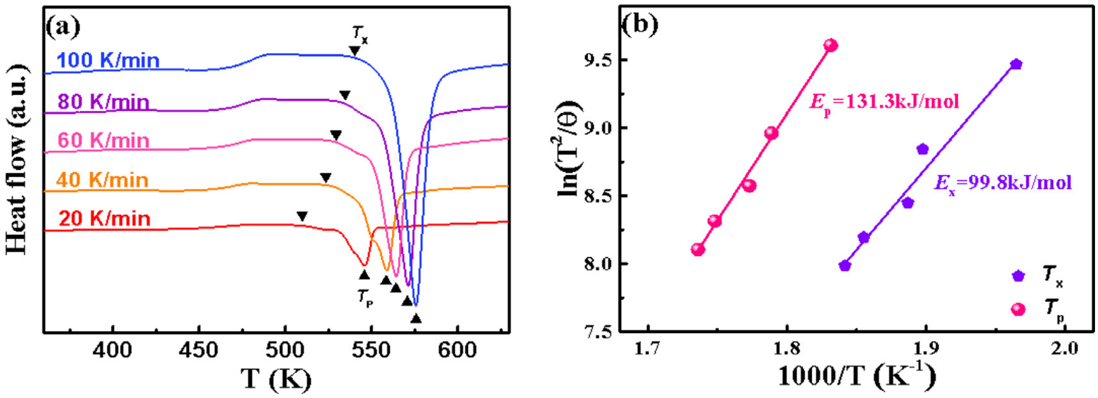

Fig. 4. The crystallization behavior of as-cast sample at different heating rates. (a) The changes in glass transition temperature T_g, crystallization onset temperature T_x and crystallization peak temperature T_p. (b) The estimation of the activation energy of the two exothermic events by using Kissinger equation.

energy exceeds a critical value about 13 J meaning partial crystallization occurred. It is consistent with above atomic structure evolution during UV process in Fig. 2. These behaviors demonstrate that the dramatically increase of T_x and ΔT in the MG below 13 J is not due to the crystallization. Actually, previous works have observed some exothermal peaks in the SLR of Pd-based glassy system, which is the consequence of a polyamorphous phase transition behavior and even leads to ultrastable MG [33,34]. Metallic glacial glass is reported to be formed by a first-order liquid-liquid transition in a LaCe-based MG, which is accompanied by a vanishment of a exothermic peak in the SLR [35]. Thus, the disappearance of the first exothermic event in Fig. 3b may be associated with some transformation behavior but not crystallization. With a suitable applied vibration energy, the ΔT can reach maximum indicating the MG system can be dramatically stabilized by UV method.

Various approaches have been used to modulate the energy state to obtain ultrastable MGs, such as high pressure (HP) [36–38], physical vapor-deposition (PVD) techniques [22,23] and sub-T_g annealing [38–41]. As a result, ΔT can be altered due to the changing of T_g or T_x. However, in most previous cases, the change in T_g is greater than T_x, resulting in a reduction of ΔT. A comparison between ΔT and other thermal parameters of this work and previous reports is summarized in Table 1. Fig. 3d displays the influence of different treatment method on the variation of ΔT. One can see that the width of ΔT keep unchanged or slightly increased when high pressure is applied to MGs, while the width of ΔT is shortened by annealing and vapor-deposition techniques. In contrast, ΔT can be remarkably increased by UV processing remarkably, an increment of 19 K or 30% achieved when the ultrasonic energy was 10 J. It means that an ultrastable supercooled liquid was achieved by UV.

To further understand the enhancement of ΔT during UV, the activation energy of the exothermic events of the as-cast sample and the UV processed sample with 10 J was evaluated. Fig. 4a presents the DSC traces of as-cast and UV processed specimens at different heating rates. Clearly there are two exothermal events exist in the as-cast specimen. The first exothermal peak is located at the left shoulder of the second main peak. After UV processing with input energy of 10 J, only the main peak is preserved. As the heating rate increasing, both T_g and T_x move to high temperature. The activation energy of the two peaks were obtained by using the Kissinger model [42], which expresses the dependence of T_x or T_p on the heating rate θ through the following equation,

$$\ln\left(\frac{T^2}{\theta}\right) = \frac{E_c}{RT} + C \tag{1}$$

where T is the temperature, R is the gas constant, E_c is activation energy and C is constant. Plotting of ln (T^2/θ) versus $1000/T$, one can get the value of the activation energy E_c from the slope (as shown in Fig. 4b). It was found that the first event has an activation energy of 98 kJ/mol, significantly lower than the second event with 133 kJ/mol. The existence of the two continuous exothermic events manifests that there are two steps during the total exothermic process. The disappearance of the first events did not affect the enthalpy ΔH_x means that the MG transforms into a lower energy state without crystallization. It is speculated that the energy input from the UV causes disappearance of the first exothermic event and the glass state transformation.

We try to understand the stabilizing of supercooled liquid state by UV from the energy point of view. We firstly evaluate the energy transfer during the UV process. As pointed out in Fig. 1b, the temperature effect during the UV treatment is very weak. Thus, it can be assumed that almost all UV input energy was absorbed by the sample. The energy density ε applied to the sample can be estimated as $\varepsilon = M \cdot U/\rho \cdot V$, where $M$is the molar mass (94.2 g/mol), U is the input energy, ρ is the density of the alloy (5.9 g/cm^3), V is the sample volume. Then, we get ε ~ 25 kJ/mol for the whole MG when the input energy is 10 J. MG consists of elastic regions and anelastic region, and only the atomic motions in the anelastic region can effectively dissipate the external energy [43]. Previous studies have found that a quarter volume of the MGs is anelastic region by using x-ray diffraction and anisotropic pair-density function analysis [44]. Thus, the energy density applied on these anelastic regions is about 100 kJ/mol, which is comparable with the activation energy of the first exothermic event. According to previous work, the activation energy (E_β) of β-relaxation of MGs follows an empirical formula $E_\beta = 26RT_g$ [45]. Here, R is gas constant. For La-based MG, the E_β is about 98 kJ/mol, which is equal to the activation energy of the first exothermic event. This indicates that the UV treatment can effectively activate β-relaxation, resulting in sufficient atomic rearrangement in the anelastic regions of flow units of MG. As a consequence, the rearrangement of the atoms in these anelastic regions induced by UV process would lead to the denser packing that is more stable state of the MG. If the input energy increases further, it will exceed the activation energy of the main crystallization event, and crystallization occurs and the crystallization enthalpies decreases as shown in Fig. 3c.

The structural evolution and the stabilization processes of the MG during the UV vibration can be schematically understood by diagram of the potential energy landscape (PEL) as displayed in Fig. 5. Generally, the PEL was used to describe the energy states of glassy materials. The energy basins and barriers on the PEL control the thermodynamics and kinetic stabilities of glass [46]. When

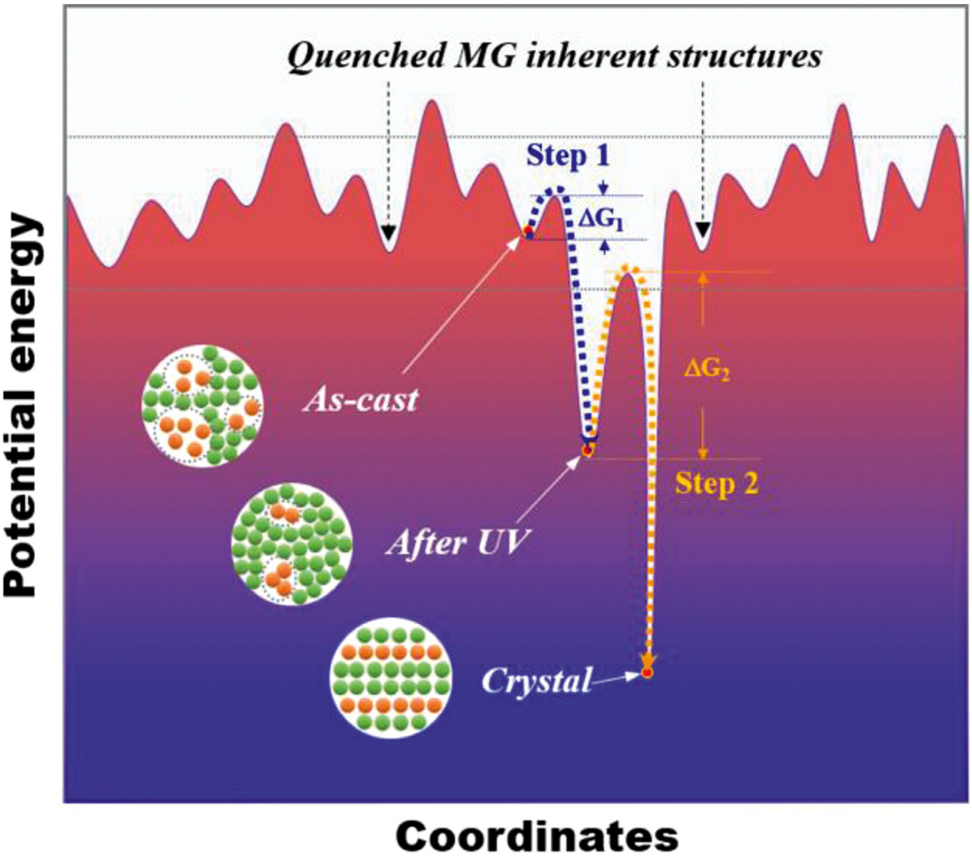

Fig. 5. Schematic diagram of the structure evolution and stabilization processes under UV in the potential energy landscape. The as cast MG quenched in a local basin with relatively higher energy. After UV at suitable energy, it can cross over an energy barrier ΔG_1 and stabilize into a denser atomic packing state. With an even larger UV energy, the MG will climb over a higher energy barrier ΔG_2 into stable crystalline state. Insets depict the atomic structure evolution after UV processing and crystallization. The orange atoms represent anelastic region that loosely pack and embed in solid glassy matrix (green atoms). (For interpretation of the references to color in this figure legend, the reader is referred to the web version of this article.) .

a system is rapidly cooled and frozen, it is usually located at an energy basin with a relatively high energy state (Quenched MG inherent structures in Fig. 5). It will evolve or thermally driven into a lower energy state, which was commonly called as relaxation [47,48]. It can also reach an even higher energy state through processes such as mechanical deformation or high pressure, which was referred as rejuvenation [48,49]. According to previous literature [44], there are plenty of liquid-like regions or anelastic regions which possess a lower activation energy in MG. Under the UV with high frequency, these loosely packed regions were activated and the atomic arrangements were enhanced, resulting in an acceleration of the relaxation process and a denser packing of these regions (its barrier ΔG_1 in PEL is about $26RT_g$, equivalent to activation energy of β-relaxation). As shown in Fig. 5, these regions tend to shrink or even disappear, which makes the MG reach a more stable state.

The enhancement of the width of SLR by UV treatment is helpful for the improvement of GFA because the width of ΔT is related to the GFA, and bulk MGs can be prepared in many system even with marginal GFA [28]. The method can also be used to achieve bulk ultrastable glass and benefit for the understanding of supercooled liquids and relaxation behavior of MGs. Moreover, the method could deliver a way to regulate crystallization to acquire glassy composite materials with controlled structure and properties.

In summary, we show the supercooled liquid of a La-based MG can be dramatically broadened and tailored by using of the high frequency ultrasonic vibration at room temperature. This makes the supercooled liquid of a glass have a higher thermal stability, namely ultrastability. The underlying physical mechanism is that some of the anelastic region or liquid-like regions in a glass can be effectively removed by the input energy of ultrasonic through the localized atomic rearrangements, and the MG then can arrive at a more stable basin in the energy landscape. The work provides a convenient route to stabilize the supercooled liquid, which would benefit for the stability and thermoplastic forming of MGs.

Declaration of Competing Interest

The authors declare no competing interests.

Acknowledgments

This work was financially supported by Guangdong Major Project of Basic and Applied Basic Research, China (Grant No. 2019B030302010), the National Key Research and Development Program of China (Grant No. 2018YFA0703604), the National Natural Science Foundation of China [Grant No. 52071222, 51871157, 11702295, 11790292, 11790291, and 61888102], the Strategic Priority Research Program of the Chinese Academy of Sciences [Grant No. XDB30000000], and the Key Research Program of Frontier Sciences [QYZDY-SSW-JSC017] .

References

[1] C.A. Angell, Science 267 (1995) 1924–1935.
[2] P.G. Debenedetti, F.H. Stillinger, Nature 410 (2001) 259–267.

[3] J.C. Dyre, Rev. Mod. Phys. 78 (2006) 953–972.
[4] X.H. Lin, W.L. Johnson, J. Appl. Phys. 78 (1995) 6514–6519.
[5] Z.P. Lu, C.T. Liu, Phys. Rev. Lett. 91 (2003) 115505.
[6] A. Peker, W.L. Johnson, Appl. Phys. Lett. 63 (1993) 2342–2344.
[7] G.J. Fan, H. Choo, P.K. Liaw, J. Non-Cryst. Solids 353 (2007) 102–107.
[8] A.L. Greer, Science 267 (1995) 1947–1953.
[9] W.L. Johnson, MRS Bull. 24 (1999) 42–56.
[10] W.H. Wang, C. Dong, C.H. Shek, Mater. Sci. Eng. R 44 (2004) 45–89.
[11] W. Klement, R.H. Willens, P. Duwez, Nature 187 (1960) 869–870.
[12] H.W. Kui, A.L. Greer, D. Turnbull, Appl. Phys. Lett. 45 (1984) 615–616.
[13] C.A. Schuh, T.C. Hufnagel, U. Ramamurty, Acta Mater. 55 (2007) 4067–4109.
[14] H.X. Li, Z.C. Lu, S.L. Wang, Y. Wu, Z.P. Lu, Prog. Mater. Sci. 103 (2019) 235–318.
[15] A. Inoue, N. Nishiyama, H. Kimura, Mater. Trans. JIM 38 (1997) 179–183.
[16] T. Waniuk, J. Schroers, W.L. Johnson, Phys. Rev. B 67 (2003) 184203.
[17] J. Schroers, Adv. Mater. 22 (2010) 1566–1597.
[18] W.H. Wang, Adv. Mater. 21 (2009) 4524–4544.
[19] T.L. Cheung, C.H. Shek, J. Alloy Compd. 434 (2007) 71–74.
[20] J.J. Lewandowski, W.H. Wang, A.L. Greer, Phil. Mag. Lett. 85 (2005) 77–87.
[21] M. Liu, C.R. Cao, Y.M. Lu, W.H. Wang, H.Y. Bai, Appl. Phys. Lett. 110 (2017) 031901.
[22] P. Luo, C.R. Cao, F. Zhu, Y.M. Lv, Y.H. Liu, P. Wen, H.Y. Bai, G. Vaughan, M. di Michiel, B. Ruta, W.H. Wang, Nat. Commun. 9 (2018) 1389.
[23] H.B. Yu, Y. Luo, K. Samwer, Adv. Mater. 25 (2013) 5904–5908.
[24] J. Eckert, J. Das, K.B. Kim, F. Baier, M.B. Tang, W.H. Wang, Z.F. Zhang, Intermetallics 14 (2006) 876–881.
[25] B.C. Wei, Y. Zhang, Y.X. Zhuang, D.Q. Zhao, M.X. Pan, W.H. Wang, W.R. Hu, J. Appl. Phys. 89 (2001) 3529–3531.
[26] A. Siddiq, E. Ghassemieh, Int. J. Adv. Manuf. Technol. 54 (2011) 997–1009.
[27] X. Li, X. Liang, Z.X. Zhang, J. Ma, J. Shen, Scr. Mater. 185 (2020) 100–104.
[28] J. Ma, C. Yang, X.D. Liu, B.S. Shang, Q.F. He, F.C. Li, T.Y. Wang, D. Wei, X. Liang, X.Y. Wu, Y.J. Wang, F. Gong, P.F. Guan, W.H. Wang, Y. Yang, Sci. Adv. 5 (2019) eaax7256.
[29] F. Sun, B. Wang, F. Luo, Y.Q. Yan, H.B. Ke, J. Ma, J. Shen, W.H. Wang, Mater. Des. 190 (2020) 108595.
[30] S. Sohrabi, M.X. Li, H.Y. Bai, J. Ma, W.H. Wang, A.L. Greer, Appl. Phys. Lett. 116 (2020) 081901.
[31] X. Liang, X. Zhu, X. Li, R. Mo, Y. Liu, K. Wu, J. Ma, Sci. China Phys. Mech. Astron. 63 (2020) 116111.
[32] M.T. Asadi Khanouki, R. Tavakoli, H. Aashuri, J. Adv. Mater. Eng. 38 (2019) 11–24.
[33] S. Lan, Y. Ren, X. Wei, B. Wang, E.P. Gilbert, T. Shibayama, S. Watanabe, M. Ohnuma, X. Wang, Nat. Commun. 8 (2017) 14679.
[34] Q. Du, X. Liu, H. Fan, Q. Zeng, Y. Wu, H. Wang, D. Chatterjee, Y. Ren, Y. Ke, P.M. Voyles, Mater. Today 34 (2019) 66–77.
[35] J. Shen, Z. Lu, J. Wang, S. Lan, F. Zhang, A. Hirata, M. Chen, X.-L. Wang, P. Wen, Y.H. Sun, J. Phys. Chem. Lett. 11 (2020) 6718–6723.
[36] R.J. Xue, L.Z. Zhao, C.L. Shi, T. Ma, X.K. Xi, M. Gao, P.W. Zhu, P. Wen, X.H. Yu, C.Q. Jin, M.X. Pan, W.H. Wang, H.Y. Bai, Appl. Phys. Lett. 109 (2016) 221904.
[37] P. Yu, H.Y. Bai, J.G. Zhao, C.Q. Jin, W.H. Wang, Appl. Phys. Lett. 90 (2007) 051906.
[38] W.H. Wang, Y.X. Zhuang, M.X. Pan, Y.S. Yao, J. Appl. Phys. 88 (2000) 3914–3918.
[39] J.Q. Wang, Y. Shen, J.H. Perepezko, M.D. Ediger, Acta Mater. 104 (2016) 25–32.
[40] M. Kohda, O. Haruyama, T. Ohkubo, T. Egami, Phys. Rev. B 81 (2010) 092203.
[41] Q. Luo, B. Zhang, D.Q. Zhao, R.J. Wang, M.X. Pan, W.H. Wang, Appl. Phys. Lett. 88 (2006) 151915.
[42] H.E. Kissinger, Anal. Chem. 29 (1957) 1702–1706.
[43] Z. Wang, W.H. Wang, Nat. Sci. Rev. 6 (2019) 304–323.
[44] W. Dmowski, T. Iwashita, C.P. Chuang, J. Almer, T. Egami, Phys. Rev. Lett. 105 (2010) 205502.
[45] H.B. Yu, W.H. Wang, H.Y. Bai, Y. Wu, M.W. Chen, Phys. Rev. B 81 (2010) 220201.
[46] F.H. Stillinger, Science 267 (1995) 1935–1939.
[47] W.H. Wang, Prog. Mater. Sci. 57 (2012) 487–656.
[48] Y.H. Sun, A. Concustell, A.L. Greer, Nat. Rev. Mater. 1 (2016) 16039.
[49] S.V. Ketov, Y.H. Sun, S. Nachum, Z. Lu, A. Checchi, A.R. Beraldin, H.Y. Bai, W.H. Wang, D.V. Louzguine-Luzgin, M.A. Carpenter, A.L. Greer, Nature 524 (2015) 200–203.